Efficient Hyperbola Detection and Fitting using Image Processing Techniques and Column-Connection Clustering

Nairit Barkataki
Dept. of Instrumentation & USIC
Gauhati University
Guwahati, India
nairitb@gauhati.ac.in

Pritha Mahanta
Dept. of Instrumentation & USIC
Gauhati University
Guwahati, India
prithamahanta21@gmail.com

Sharmistha Mazumdar
Dept. of Instrumentation & USIC
Gauhati University
Guwahati, India
sharmistha.13ghy@gmail.com

Utpal Sarma
Dept. of Instrumentation & USIC
Gauhati University
Guwahati, India
utpalsarma@gauhati.ac.in

***Abstract*—Ground Penetrating Radar (GPR) is a preferred non-destructive method used for the identification and localisation of subsurface targets. Hyperbolic signatures present in GPR B-Scans can provide valuable insights about the shape, material and the distance at which target objects are buried below the surface. This paper presents an innovative approach to enhance GPR data analysis, specifically focusing on hyperbola detection within GPR B-Scans. Preprocessing steps, such as dewow filtering, frequency filtering, and gain compensation, are used to improve GPR data quality. A comparative analysis is conducted on the performance of Canny, Sobel, and Scharr edge detectors in identifying hyperbolic signatures. By merging the Canny edge detection algorithm with the Column-Connection Clustering (C3) method, common limitations of conventional clustering, particularly their sensitivity to noise and outliers are addressed. Finally, the efficacy of the proposed method is evaluated by calculating the R-squared values of the fitted hyperbolas which was found to be > 0.93.**

***Index Terms*—ground penetrating radar, edge detection algorithm, hyperbola detection, column-connection clustering (C3), sub-surface imaging**

I. Introduction

Ground penetrating radar (GPR) employs electromagnetic waves to look beneath the surface of the earth [1]. A-Scan is a one-dimensional representation of GPR data, which is formed by capturing the time-series of the reflected wave signals. B-Scan is a two-dimensional representation of the data which is formed when several A-Scans are collected along a specific direction [2].

GPR is used in numerous fields for various applications like road inspection, bridge assessment, underground utility evaluation [3], landmine detection [4], non-destructive survey of archaeological sites [5] etc. GPR enables the non-destructive evaluation of various structures and helps ensure their integrity and safety [3].

II. Literature Review

The scattering of transmitted pulses from buried objects create hyperbolic features within GPR B-Scans. Unprocessed GPR data can provide a detailed map of the shallow subsurface, but interpreting this data accurately can be challenging. However, by applying different signal processing techniques, the standard of GPR images from the test site can be greatly enhanced. Multiple methods employed for processing the signals include filtering techniques to remove low frequency components (dewow) [6], applying gain, time-zero correction, migration, bandpass filtering, background removal and velocity analysis [7], [8].

The implementation of the pre-processing techniques is usually followed by the implementation of edge detectors. This further enhances the GPR images and accurately traces the edges of the hyperbolic features. Canny [9] and Sobel [4] filters are two widely used edge detectors.

Hyperbolic features signify the existence of buried items such as cables, pipelines, geological formations, historical relics, and even explosive devices [10]. The task of recognising and pinpointing these hyperbolic patterns becomes imperative for proper interpretation of GPR data. Following detection, appropriate techniques are applied to fit the identified hyperbolas. The fitted hyperbolas provide diverse insights, encompassing target recognition [11], depth estimation [12], and determination of target dimensions [13], among others.

Numerous approaches have been suggested for detecting the hyperbolas present in GPR B-Scans. Altin et al. implemented Otsu thresholding and Hough transformation to extract soil planes in GPR B-Scans [14]. Curve-fitting techniques in conjunction with neural networks have also been employed to detect buried objects and estimate their positions [15].

Various clustering algorithms like the column-connection

clustering (C3) algorithm [16], open-scan clustering algorithm, double cluster seeking estimate [17], slice-connection clustering algorithm [18] are employed to detect the hyperbolic signatures. The column-connection clustering (C3) algorithm detects regions in GPR data that potentially contain hyperbolas. These regions are subsequently categorised into clusters. In the study by Dou et al. an adaptive thresholding algorithm was utilised to distinguish the potential hyperbola-containing regions from the background [16]. Subsequently, the C3 algorithm was employed to differentiate the identified regions from each other. Hough transform and C3 algorithm were utilised by Kafedziski et al. to detect hyperbola and estimate the precise target depth on data obtained from the Web and simulation using gprMax [19]. Wunderlich et al. used RetinaNet, a deep learning model for automated detection of hyperbolas [20]. The accuracy of the detected hyperbolas was verified by assessing them in relation to manual determinations of velocities and apex points. The findings indicated that the most efficient approach for extracting hyperbolas involved utilising a threshold and the C3 algorithm, followed by a direct hyperbola fitting process.

While the clustering algorithms specified have been employed to detect hyperbolic signatures in various contexts, including GPR data analysis, there exist multiple drawbacks associated with their usage. Clustering algorithms can be sensitive to noisy or outlier data points. Given the existence of noise, the clustering results may be distorted, leading to inaccurate detection of hyperbolic signatures. Outliers, if not handled properly, can also disrupt the clustering process and affect the formation of meaningful clusters. Edge detection algorithms emphasise the boundaries between different materials or subsurface layers. By accentuating the edges, these algorithms can improve the visual interpretation of the GPR data, making it easier to identify and understand the subsurface structures.

This study presents an innovative approach by integrating the Canny edge detection algorithm along with C3 algorithm to identify the presence of hyperbolas in GPR B-Scans.

III. GPR Data Collection

The dataset employed in this study was collected at the Geosciences and Technology division in NEIST (Jorhat). A commercial GPR sytem (pulseEKKO PRO) was utilised for the data collection. In total, 151 A-Scans were recorded, each having 250 samples. The separation between the transmitter and receiver antennas was 0.5 m and were operated at a centre frequency of 200 MHz. The GPR B-Scan image is shown in Figure 1.

IV. Methodology

This section describes the various preprocessing techniques employed in this study. Python programming language is used to implement these techniques.

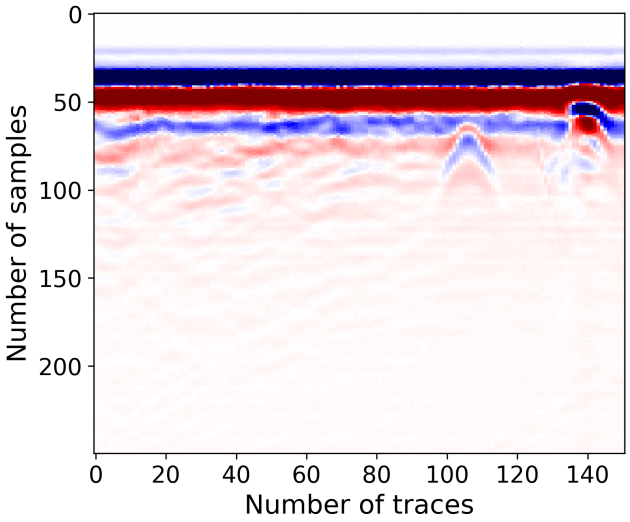

Fig. 1: Plot of unprocessed GPR data

A. Dewow

The GPR A-Scan contains a low-frequency component called the ‘wow’ that originates from various factors like the separation between the transmitter and receiver and the ground’s electrical properties. This ‘wow’ effect is characterised by a sudden onset, reaching a peak, and subsequently decaying exponentially [6]. It is present in every raw radar recording and appears alongside the higher frequency reflections in the data. Dewow filtering is the removal of the low-frequency component.

This work applies an average subtraction filter to eliminate the wow component. This filter operates differently in accordance with the window size relative to the overall quantity of samples. In this study, the dimensions of the window is considered to be less than the total count of samples. The average of half the window size is subtracted from each sample of every A-Scan. The resulting information is stored in a new matrix. By applying this technique, the low-frequency wow component is effectively removed, allowing for data normalisation and facilitating the utilisation of positive and negative colour filling in the displayed traces.

B. Frequency filtering

To improve the visual quality of the data and remove unwanted noise, various filters can be put to use on the GPR B-Scans to enhance the clarity of the information and aid in the interpretation process.

A spatial median filter is applied in this work. This filter operates on each sample of the B-Scan by selecting neighbouring samples within a specified window. As the window slides through the B-Scan, the median value of the samples within the window is computed. The median value is calculated by sorting the neighbouring samples in ascending order and selecting the middle value. The current sample in the B-Scan is then replaced with the calculated median value. This procedure is iterated for all samples in the B-Scan image. The median

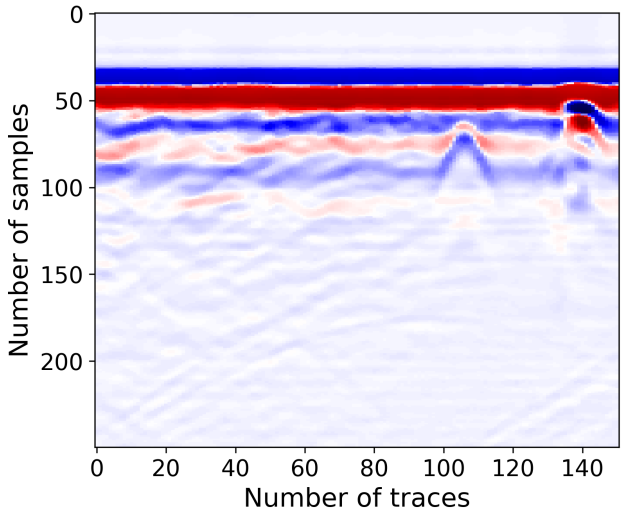

Fig. 2: GPR B-Scan after applying dewow, frequency filtering and gain

filter is particularly effective in removing impulsive noise or outliers from the signal.

C. Gain

As the GPR signal propagates through the ground, certain portions of the reflected signal become attenuated or lost. This causes the signal to weaken as the depth increases. To address this issue, compensating gain is applied to the data. This enhances the visibility of all targets as much as possible without amplifying the inherent presence of noise in the data. In this study, power gain is used. Mathematically, it can be depicted by the equation:

$$x_g(n) = x(n) \times n^{\alpha} \tag{1}$$

Here, α is a parameter that needs to be selected. $x_g(n)$ represents the sample obtained after applying the gain. The gain is calculated by raising the sample index (n) to the power of α. The processed image at this stage is shown in Figure 2.

D. Feature Extraction

Edge detection is an essential image processing method employed to detect and highlight borders or edges of objects within an image. The purpose of performing edge detection is to extract important information from an image by locating abrupt changes in intensity or colour, which typically correspond to object boundaries or transitions between different regions within the image. Canny, Sobel and Scharr edge detection algorithms are used in this work.

It is observed that Canny edge detector yields better results than Sobel and Scharr methods. This is due to its accurate localisation, low error rate, robustness to noise, and ability to provide single edge responses. The Figure 3 illustrates a sequence of images showcasing a GPR B-Scan along with the outcomes of Canny, Sobel, and Scharr edge detection algorithms applied to the GPR B-Scan data.

E. Column-Connection Clustering (C3) Algorithm

After the edges are detected in the image, C3 algorithm is used to segregate the regions that potentially contain hyperbolas. The C3 algorithm consists of two crucial components: Column segment and Connecting elements.

Column segment: A Column segment refers to a consecutive set of points along a column in the image. To be recognised as a column segment, the count of successive points within the cluster must meet or exceed a predetermined threshold value (in this work, 3). The purpose of setting this threshold is to effectively filter out noise and ensure that the segment contains meaningful information.

Connecting elements: Connecting elements refer to the points within a column segment that share the same row number. When two column segments adjacent to each other have connecting elements, it indicates that they have points in common along the same row. In the C3 algorithm, the elements of adjacent column segments in neighbouring columns are compared. If connecting elements are found, the cluster extends to the next column, incorporating the elements from the subsequent column segment. This process is carried on for all columns, generating clusters in accordance with the connections between columns.

In short, the C3 algorithm analyses the columns of the image by detecting column segments and connecting elements to create clusters. It commences with the initial column and extends the clusters to subsequent columns if there are connecting elements present. This repetitive process carries on until all columns have been examined, which culminates in the establishment of distinct clusters in accordance with

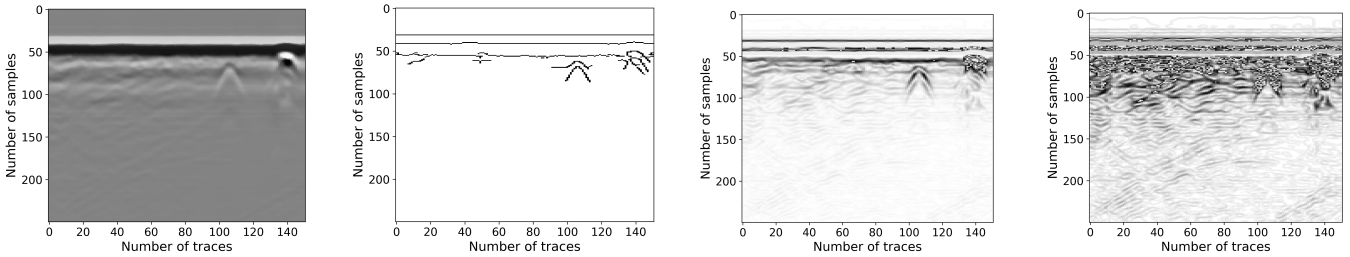

Fig. 3: (a) Original GPR Image, (b) Post-Canny Edge Detection, (c) Post-Sobel Edge Detection, (d) Post-Scharr Edge Detection

the connections between columns. Figure 4 demonstrates the identification of a hyperbolic pattern within a GPR B-Scan image by implementing the C3 algorithm.

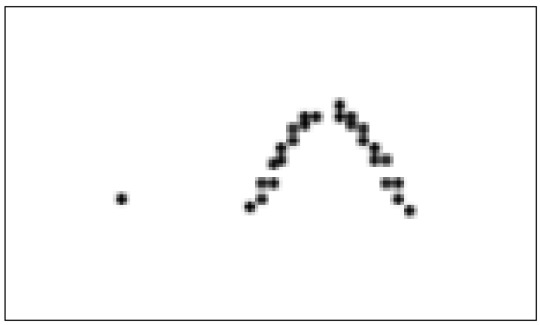

Fig. 4: Detected hyperbola in GPR B-Scan image using C3 algorithm

F. Hyperbola Fitting

In GPR data interpretation, hyperbola fitting helps in identifying and distinguishing various subsurface targets based on their hyperbolic signatures. In addition to that, it offers a way to estimate the depth of buried targets. In this paper, the hyperbola has been fitted using the standard equation of a hyperbola:

$$\frac{(y-n)^2}{\alpha^2} - \frac{(x-m)^2}{\beta^2} = 1, \tag{2}$$

where *(m,n)* represents the centre of the hyperbola, α represents the semi-major axis and β represents the semi-minor axis. The coordinates of the hyperbolic feature obtained from the C3 algorithm are used for hyperbola fitting.

V. Results

The proposed method for fitting hyperbola is first applied on the GPR B-Scan data collected in the laboratory. Figure 5 shows the accurate fitting of hyperbola onto the GPR B-Scan data.

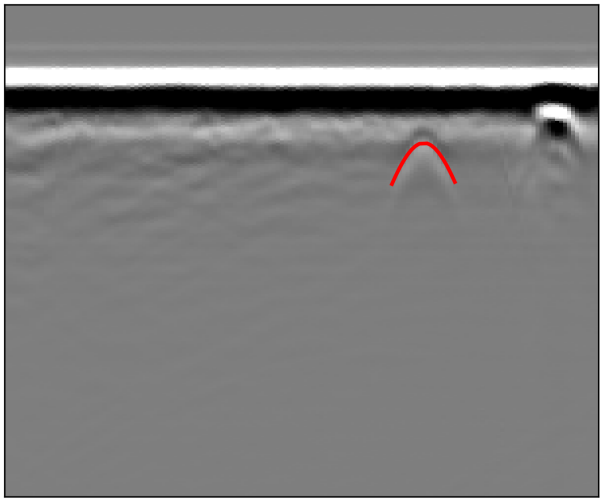

Fig. 5: Hyperbola fitting on GPR B-Scan data

To evaluate the extent to which the fitted curve accurately captures the changes seen within the actual data points, the R-squared (R^2) metric is calculated using the following formula:

$$R^2 = 1 - \frac{SS_{\text{res}}}{SS_{\text{tot}}} \tag{3}$$

where, SS_{res} (sum of squares of residuals) represents the sum of the squared differences between the actual values and the predicted values from the fitted curve and SS_{tot} (total sum of squares) denotes the sum of the squared differences between the actual data points and the mean of all the predicted values.

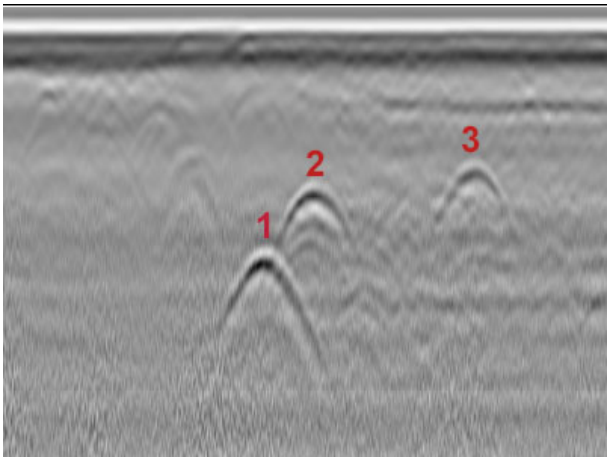

Fig. 6: B-Scan *Image A* having multiple hyperbolic features used for the verification of the algorithm

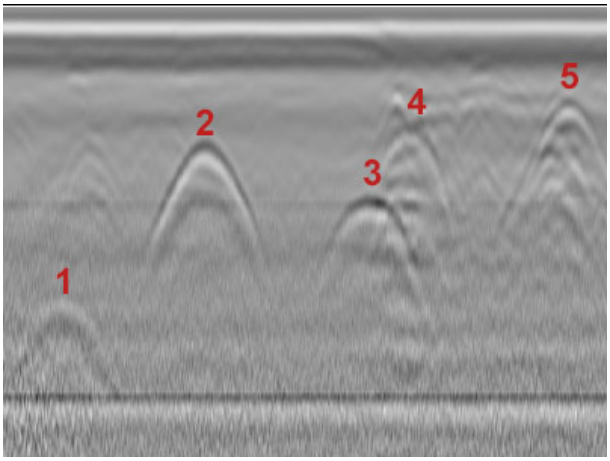

Fig. 7: B-Scan *Image B* having hyperbolic features used for the verification of the algorithm

The R^2 value achieved for the fitted hyperbola in Figure 5 is 0.949. As the R^2 value is observed to be closer to 1, it denotes that a bigger amount of the variance in the data points is explained by the fitted curve, suggesting a good fit between the curve and the data points.

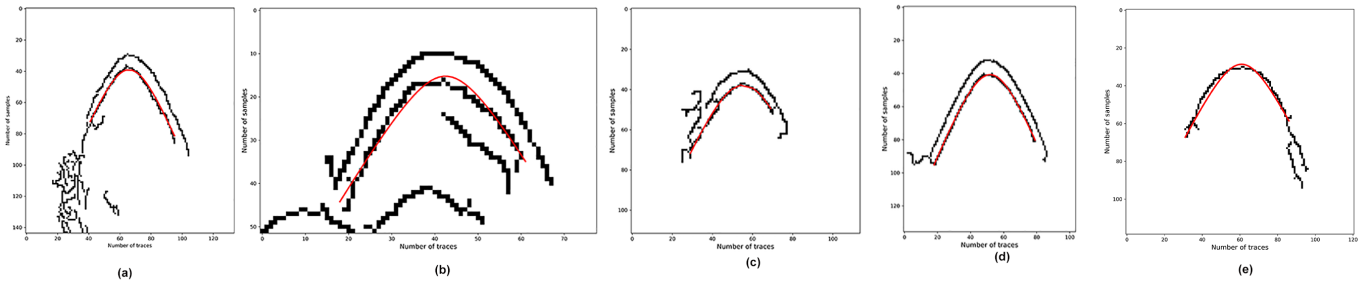

Fig. 8: Fitted hyperbolas for the B-Scan images used for validation

A. *Validation of the proposed algorithm*

To verify the performance of the proposed method for fitting hyperbolas, it was further applied on 2 different B-Scan images shown in Figure 6 (*Image A*) and Figure 7 (*Image B*) obtained from the data collected by [16]. The algorithm is applied to hyperbolas marked as 1, 2 and 3 in *Image A*, and the fitted hyperbolas for this image are shown in Figure 8 (a), (b) and (c) respectively. Further, the algorithm is also employed for the hyperbolas marked as 2 and 3 in *Image B* and the fitted hyperbolas are shown in Figure 8 (d) and (e) respectively.

Table I shows a comparison of the R^2 values obtained for the hyperbolas fitted using the proposed method.

TABLE I: Comparison of R^2 values for the fitted hyperbolas

Sl. No.	**Hyperbola**	R^2 **value**
1	Hyperbola 1 of Image A	0.939
2	Hyperbola 2 of Image A	0.942
3	Hyperbola 3 of Image A	0.971
4	Hyperbola 2 of Image B	0.995
5	Hyperbola 3 of Image B	0.949

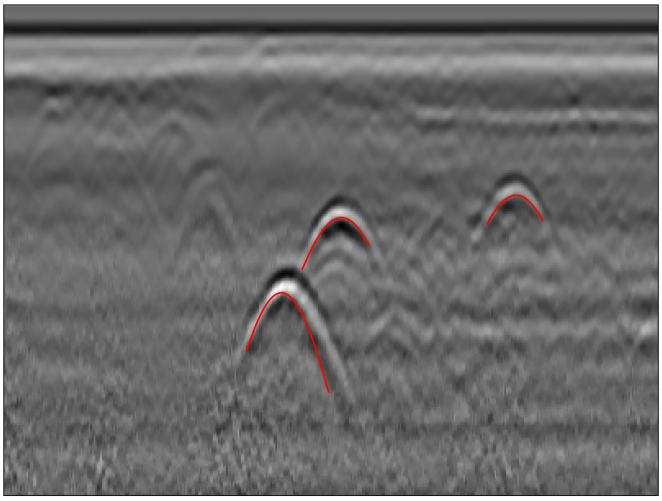

Fig. 9: B-Scan image shown in Figure 6 with the fitted hyperbolas

The proposed method's performance is quantified by R^2 values, a metric that gauges the goodness of fit. For *Image A*, we obtained R^2 values of 0.939, 0.942, and 0.971 for hyperbolas 1, 2, and 3, respectively. When considering *Image B*, hyperbolas 2 and 3 yielded R^2 values of 0.995 and 0.949, affirming the accuracy and robustness of our method in capturing the hyperbolic signatures across diverse datasets.

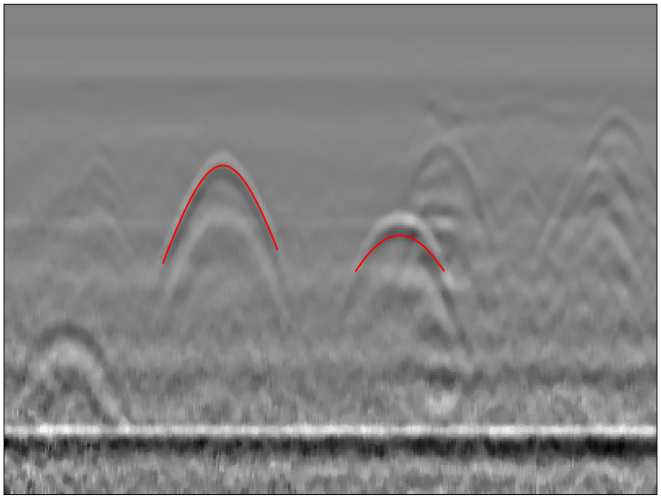

Fig. 10: B-Scan image shown in Figure 7 with the fitted hyperbolas

In Figures 9 and 10, a visual representation of the outcomes of our verification process is provided. These figures illustrate the fitted hyperbolas overlaid on the original GPR B-Scan images, further corroborating the reliability and effectiveness of our proposed algorithm. These results collectively affirm the versatility and robustness of our method, which shows potential for a range of applications, including subsurface structure analysis and target localisation.

VI. Conclusion

In this study, a novel approach was presented integrating the Canny edge detection algorithm with the C3 algorithm for hyperbola detection in GPR B-Scans. The integration of these techniques addressed certain constraints linked to conventional clustering algorithms, particularly their sensitivity to noisy data and outliers. The proposed methodology involved several preprocessing steps, including dewow filtering, frequency filtering, and gain compensation, to improve the quality of

GPR data. Additionally, edge detection algorithms, specifically Canny, Sobel, and Scharr, were used to identify object boundaries and improve the visual interpretation of subsurface structures. It was seen that Canny outperformed the other edge detectors and hence it was finally used before applying the C3 algorithm.

The core of this approach lies in the application of Canny edge detector with the C3 algorithm, which effectively segregates regions potentially containing hyperbolic signatures. Subsequently, a suitable hyperbola fitting technique was employed. The validation of this method on different datasets demonstrated its robustness and versatility. High R^2 values were achieved, indicating the accuracy of our hyperbola fitting process. Figures 8, 9, and 10 visually confirmed the precise alignment of hyperbolas on GPR B-Scan images. The results underscore the potential of this approach in diverse applications, including subsurface structure analysis and target localisation. By mitigating the limitations associated with traditional clustering algorithms, this method offers a promising avenue for enhancing the interpretation of GPR data and advancing subsurface imaging technologies.

VII. Acknowledgement

The authors convey their profound gratitude to NEIST (Jorhat), with special appreciation for the invaluable support provided by Dr. Manoj Kumar Phukan and Mr. Sausthov M. Bhattacharyya during the GPR data collection process. The authors acknowledge Ankur Jyoti Kalita for his help during the implementation of the preprocessing algorithms.

References

[1] R. Persico, *Introduction to ground penetrating radar: inverse scattering and data processing*. John Wiley & Sons, 2014.

[2] S. Kanafiah, H. Ali, A. A. Firdaus, M. Z. Azalan, Y. Jusman, A. Khairi, M. Ahmad, T. Sara, T. Amran, I. Mansor *et al.*, "Metal shape classification of buried object using multilayer perceptron neural network in gpr data," in *IOP Conference Series: Materials Science and Engineering*, vol. 705, no. 1. IOP Publishing, 2019, p. 012028.

[3] W. W.-L. Lai, X. Derobert, and P. Annan, "A review of ground penetrating radar application in civil engineering: A 30-year journey from locating and testing to imaging and diagnosis," *Ndt & E International*, vol. 96, pp. 58–78, 2018.

[4] N. Barkataki, B. Tiru, and U. Sarma, "A cnn model for predicting size of buried objects from gpr b-scans," *Journal of Applied Geophysics*, vol. 200, p. 104620, 2022.

[5] E. Corradini, D. Groß, T. Wunderlich, H. Lübke, D. Wilken, E. Erkul, U. Schmölcke, and W. Rabbel, "Finding mesolithic sites: a multichannel ground-penetrating radar (gpr) investigation at the ancient lake duvensee," *Remote Sensing*, vol. 14, no. 3, p. 781, 2022.

[6] K. Gerlitz, M. D. Knoll, G. M. Cross, R. D. Luzitano, and R. Knight, "Processing ground penetrating radar data to improve resolution of near-surface targets," in *6th EEGS Symposium on the Application of Geophysics to Engineering and Environmental Problems*. European Association of Geoscientists & Engineers, 1993, pp. cp–209.

[7] A. Benedetto, F. Tosti, L. B. Ciampoli, and F. D'amico, "An overview of ground-penetrating radar signal processing techniques for road inspections," *Signal processing*, vol. 132, pp. 201–209, 2017.

[8] L. Bianchini Ciampoli, F. Tosti, N. Economou, and F. Benedetto, "Signal processing of gpr data for road surveys," *Geosciences*, vol. 9, no. 2, p. 96, 2019.

[9] Ž. Bugarinović, L. Pajewski, A. Ristić, M. Vrtunski, M. Govedarica, and M. Borisov, "On the introduction of canny operator in an advanced imaging algorithm for real-time detection of hyperbolas in ground-penetrating radar data," *Electronics*, vol. 9, no. 3, p. 541, 2020.

[10] F. J. Alcalá, P. Martínez-Pagán, M. C. Paz, M. Navarro, J. Pérez-Cuevas, and F. Domingo, "Combining of masw and gpr imaging and hydrogeological surveys for the groundwater resource evaluation in a coastal urban area in southern spain," *Applied Sciences*, vol. 11, no. 7, p. 3154, 2021.

[11] L. Qiao, Y. Qin, X. Ren, and Q. Wang, "Identification of buried objects in gpr using amplitude modulated signals extracted from multiresolution monogenic signal analysis," *Sensors*, vol. 15, no. 12, pp. 30 340–30 350, 2015.

[12] F. Xie, W. W. Lai, and X. Dérobert, "Gpr-based depth measurement of buried objects based on constrained least-square (cls) fitting method of reflections," *Measurement*, vol. 168, p. 108330, 2021.

[13] W. Lei, J. Luo, F. Hou, L. Xu, R. Wang, and X. Jiang, "Underground cylindrical objects detection and diameter identification in gpr b-scans via the cnn-lstm framework," *Electronics*, vol. 9, no. 11, p. 1804, 2020.

[14] G. ALTIN and A. DOLMA, "Buried objects segmentation and detection in gpr b scan images," *The Eurasia Proceedings of Science Technology Engineering and Mathematics*, vol. 6, pp. 11–17, 2019.

[15] N. P. Singh and M. J. Nene, "Buried object detection and analysis of gpr images: Using neural network and curve fitting," in *2013 Annual International Conference on Emerging Research Areas and 2013 International Conference on Microelectronics, Communications and Renewable Energy*. IEEE, 2013, pp. 1–6.

[16] Q. Dou, L. Wei, D. R. Magee, and A. G. Cohn, "Real-time hyperbola recognition and fitting in gpr data," *IEEE Transactions on Geoscience and Remote Sensing*, vol. 55, no. 1, pp. 51–62, 2016.

[17] W. Lei, F. Hou, J. Xi, Q. Tan, M. Xu, X. Jiang, G. Liu, and Q. Gu, "Automatic hyperbola detection and fitting in gpr b-scan image," *Automation in Construction*, vol. 106, p. 102839, 2019.

[18] W. Luo, Y. H. Lee, L. F. Ow, M. L. M. Yusof, and A. C. Yucel, "Slice-connection clustering algorithm for tree roots recognition in noisy 3d gpr data," in *2022 IEEE USNC-URSI Radio Science Meeting (Joint with AP-S Symposium)*. IEEE, 2022, pp. 122–123.

[19] V. Kafedziski, S. Pecov, and D. Tanevski, "Target detection in sfcw ground penetrating radar with c3 algorithm and hough transform based on gprmax simulation and experimental data," in *2018 25th International Conference on Systems, Signals and Image Processing (IWSSIP)*. IEEE, 2018, pp. 1–5.

[20] T. Wunderlich, D. Wilken, B. S. Majchczack, M. Segschneider, and W. Rabbel, "Hyperbola detection with retinanet and comparison of hyperbola fitting methods in gpr data from an archaeological site," *Remote Sensing*, vol. 14, no. 15, p. 3665, 2022.